261 (2026) 214433

Contents lists available at ScienceDirect

Geoenergy Science and Engineering

journal homepage: www.sciencedirect.com/journal/geoenergy-science-and-engineering

Experiment-supported simulation of silica nanofluid alternating CO_2 injection: Sensitivity analysis for enhanced oil recovery and CO_2 storage in sandstone reservoirs

Ragheed Alali *, Kazunori Abe **, Hikari Fujii

Department of Earth Resource Engineering and Environmental Science, Graduate School of International Resource Sciences, Akita University, 1–1 Tegata Gakuen-Machi, Akita 010-8502, Japan

A R T I C L E I N F O

Keywords:
Nanofluid alternating gas injection
Carbon storage
Enhanced oil recovery
Silica nanoparticles
Reservoir simulation

A B S T R A C T

Water-based nanofluid alternating gas (NWAG) injection is a promising approach for enhancing oil recovery in carbonate and sandstone reservoirs. The NWAG injection performance is influenced by multiple parameters, which necessitates sensitivity analysis using computer simulation. NWAG simulations have been reported for carbonate reservoirs. However, in sandstone, the NWAG method has only been studied through laboratory experiments. This study aims to investigate the reliability of the NWAG method in sandstone on a large scale by making a simulation and performing sensitivity analysis for the slug size, NWAG ratio, and nanoparticle concentration in a three-dimensional model of a sandstone reservoir. Silica nanofluid and CO_2 were chosen to investigate oil recovery and CO_2 storage performance during NWAG injection. A reservoir-scale model was constructed by upscaling a laboratory-validated one-dimensional model based on a core flooding experiment. Subsequently, several simulations were performed to determine the effects of each parameter. Results indicated that a slug size of 0.2 hydrocarbon pore volume, NWAG ratio of 1:1, and nanoparticle concentration of 0.5 wt% resulted in the fastest oil recovery. Moreover, results suggested that nanofluid plays two equally important roles, controlling gas mobility and altering rock wettability, and focusing only on one aspect leads to inferior results. For CO_2 storage, larger slug sizes and higher gas ratios resulted in greater CO_2 storage but at the expense of longer operation time for the same amount of oil produced. Overall, the study findings demonstrate that by using the right parameters, NWAG injection can be effective for simultaneous oil recovery and CO_2 storage in sandstone reservoirs.

Abbreviations

NPs	Nanoparticles
NF	Nanofluid
IFT	Interfacial tension
WAG	Water alternating gas
NWAG	Water-based nanofluid alternating gas
SiO_2	Silicon dioxide (silica)
CMG	Computer Modelling Group
FW	Formation water
HCPV	Hydrocarbon pore volume

1. Introduction

The global demand for energy, driven by developing economies, is continually rising. Despite rapid growth of renewable energy sources and their increased share of the energy supply, demand for fossil fuels has not yet peaked and is not expected to do so for many years (IEA, 2024). Therefore, oil and gas production should grow in tandem with meeting global needs, especially in regions where access to other reliable energy sources remains limited.

Substantial amounts of oil remain unrecovered after primary and secondary oil recovery stages, and enhanced oil recovery techniques have been designed to tap into residual oil reserves. Each of these techniques utilizes different mechanisms in accordance with specific

* Corresponding author.
** Corresponding author.
E-mail addresses: ragheedalali@hotmail.com (R. Alali), abe@mine.akita-u.ac.jp (K. Abe).

https://doi.org/10.1016/j.geoen.2026.214433
Received 12 September 2025; Received in revised form 27 November 2025; Accepted 20 February 2026
Available online 21 February 2026

reservoir conditions. Among them, using nanoparticles (NPs) in enhanced oil recovery has emerged as an interesting technique that leverages oil–nanoparticle and rock–nanoparticle interactions to increase oil production (Deshmukh and Pathan, 2025; Kandiel et al., 2025; Liang et al., 2025; Ogolo et al., 2012).

NPs are solid particles ranging from 1 to 100 nm in diameter. In enhanced oil recovery, NPs are mixed with a base fluid to create a colloidal solution, known as a nanofluid (NF), that can be injected into the oil reservoir. The interest in NPs as enhanced oil recovery agents began in the early 2010s and grew steadily ever since. Several types of NPs have proven their effectiveness in this application, such as aluminum oxide (Al_2O_3), titanium dioxide (TiO_2), and silicon dioxide (silica, SiO_2) (Alsaba et al., 2020; Hogeweg et al., 2018; Ogolo et al., 2012), and they were applied to both carbonate (Esfandyari Bayat et al., 2014) and sandstone (Ehtesabi et al., 2014). However, SiO_2 NPs attracted more interest due to their potency as an enhanced oil recovery agent and for being more environmentally friendly (Kandiel et al., 2025; Ogolo et al., 2012). This interest was reflected by the large number of publications discussing SiO_2 compared to other types of NPs (Alsaba et al., 2020).

NF injection can increase oil production through several mechanisms, as shown in Fig. 1, including reducing interfacial tension (IFT) between oil and water, pore plugging that causes flow paths to diverge into untapped regions, altering surface wettability to a more water-wet state, and creating disjoining pressure that removes oil from the rock surface (Abe et al., 2023; Deshmukh and Pathan, 2025; Kandiel et al., 2025; Liang et al., 2025; Sun et al., 2024). Although NF injection has negative aspects such as permeability damage (Alali et al., 2023; Esfandyari Bayat et al., 2015), this method has attracted increasing attention among researchers in recent years, with over half of NPs enhanced oil recovery studies published between 2020 and 2024 (Kandiel et al., 2025). Moreover, the drawbacks of NF injection have not prevented a field application of this method (Kumasaka et al., 2024).

Another prominent enhanced oil recovery method is CO_2 injection. A plethora of studies have proven that CO_2 injection improves oil recovery by dissolving CO_2 in oil, expanding the oil volume and reducing its viscosity (Abdulsada et al., 2025; Cao et al., 2021; Fang et al., 2024; Luo et al., 2017). However, viscous fingering and gravity segregation, arising from the vast property differences between CO_2 and oil, hinder the efficiency of this method. To overcome these challenges, water alternating CO_2 (WAG) injection was developed to reduce the mobility of CO_2 (Abdulsada et al., 2025; Cao et al., 2021; Fang et al., 2024; Ren et al., 2023; Sun et al., 2024). This method was later augmented by replacing water with a water-based NF, resulting in water-based NF alternating CO_2 (NWAG) injection (Aziz et al., 2021; Cao et al., 2021; Hu et al., 2023; Moradi et al., 2015).

NWAG injection was first introduced by (Moradi et al., 2015) to improve the effectiveness of conventional WAG injection in carbonate reservoirs, which tend to have more oil-wet than water-wet characteristics. Multiple studies comparing NWAG and WAG injections have demonstrated that NWAG injection always results in a higher oil recovery factor (Al Matroushi et al., 2015; Hu et al., 2023; Ko et al., 2024; Moradi et al., 2015). Wettability alteration is not the only effect induced by NFs, and the NWAG process eventually proved to be beneficial in sandstone mediums (Cao et al., 2021; Hu et al., 2023), albeit with not extensive wettability change owing to the already water-wet nature of sandstone (Zhang et al., 2023). Furthermore (Cao et al., 2021; Hu et al., 2023), reported the synergetic effects of using NFs with CO_2 during the NWAG process, such as lowering the heavy component content of oil, thereby enhancing the interaction between CO_2 and oil and improving the flooding process. Additionally, when focusing not only on oil recovery but also on CO_2 storage, several studies reported that silicon dioxide/silica (SiO_2) NF absorbed more CO_2 than water through increased solubility, diffusion (Rahmatmand et al., 2016; Sun et al., 2023), and adsorption of CO_2 on the NP surface (Vittoni et al., 2019). Consequently, this method is ideal for nearly depleted oil reservoirs as it enables simultaneous and efficient oil recovery and CO_2 storage.

Owing to its many parameters, choosing the wrong values can lower the efficiency of NWAG injection. Therefore, understanding the effects of each of these parameters on the NWAG injection outcome is necessary. Parameter sensitivity analysis can be costly, laborious, and time consuming if done through laboratory experiments. Hence, simulations of this process were eventually created to simplify the process (Al Matroushi et al., 2015). and (Ko et al., 2024) published simulations of SiO_2 NPs and CO_2 NWAG injection in carbonate reservoirs. (Al Matroushi et al., 2015), employing Eclipse100 software, reported that a 6 months cycle with 5 months of NF injection and 1 month of CO_2 injection at a 2:1 NWAG ratio resulted in an optimal oil recovery factor

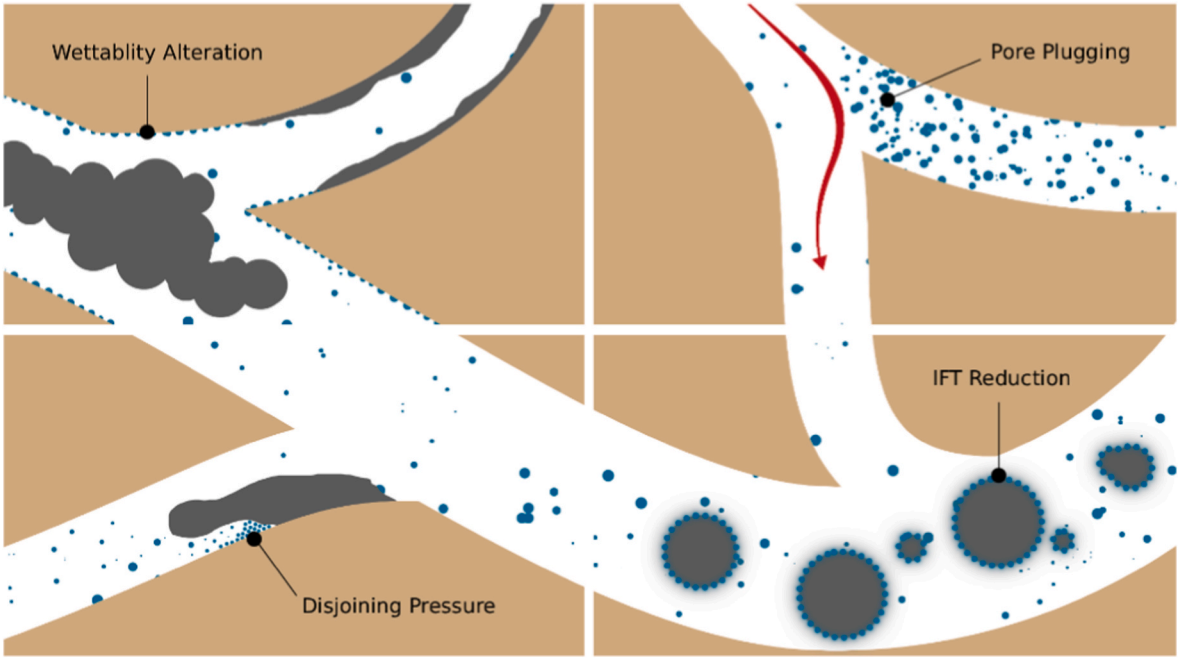

Fig. 1. Different mechanisms of NPs enhanced oil recovery.

that was 13% higher than that of WAG injection. Using Computer Modelling Group (CMG) GEM software and focusing on CO_2 storage after NWAG injection in a heterogeneous carbonate reservoir (Ko et al., 2024), reported a 0.8% increase in the oil recovery factor and 15.2% increase in the amount of stored CO_2 compared to WAG injection.

The aforementioned simulation studies have demonstrated the reliability of the NWAG method in carbonate reservoirs. However, because the wettability alteration and mobility control benefits of NF are more prominent in heterogeneous carbonate reservoirs, the question of whether the NWAG method would be effective in sandstone reservoirs remains insufficiently addressed in prior studies. Therefore, the simulation presented in this study focuses on the application of NWAG injection in a sandstone reservoir and the benefits of this method in terms of simultaneous oil recovery and CO_2 storage. A reservoir-scale model was constructed using CMG simulation software by upscaling a laboratory-scale model, and several simulations were conducted with various slug sizes, NWAG ratios, and NP concentrations to optimize for maximum oil recovery and CO_2 storage. Moreover, the method used herein for simulating NPs behavior in CMG relied on the Petronas AFM (Nanoparticle) Wizard that was not used in previous NWAG studies.

2. Methodology

The creation of a three-dimensional (3D) reservoir-scale simulation began with a one-dimensional (1D) laboratory-scale simulation. The 1D model was based on a core flooding experiment. After satisfactorily matching experimental and simulation results, the 1D model was upscaled to the reservoir scale. The following sections discuss the materials utilized in the experiments and methods employed to collect the data required for model creation.

2.1. Materials

SiO_2 NF was obtained from Nissan Chemical Corporation (Tokyo, Japan). The NPs were spherical with an average diameter of 22 nm after preparation, as shown in Fig. 2. The NF was diluted to a concentration of 0.5 wt% using a base fluid of synthetic formation water (FW) with a salinity of 18,000 ppm. The synthetic FW was based on FW in the field where the crude oil was sourced, and its contents are presented in Table 1.

Crude oil viscosity was measured using a DV2T viscometer (Brookfield, Middleboro, MA, USA) and FW and NF viscosities were measured using an SV-10 Sine-wave Vibro viscometer (A&D Company, Ltd., Tokyo, Japan). All fluid densities were measured using a hydrometer. The measured properties of the crude oil, FW, and NF are presented in Table 2.

The core sample was Berea Buff sandstone obtained from Kocurek Industries, Inc. (Caldwell, TX, USA). The porosity and permeability of the sample were measured using a PoroPerm apparatus (Vinci Technologies, Nanterre, France) before saturating the core sample with FW using a vacuum chamber. Following FW saturation, the core was saturated with oil using an SRP350 core flooding apparatus (Vinci Technologies, Nanterre, France), as shown in Fig. 3. According to (Al-Ameer et al., 2023), sandstone samples require 2-3 weeks of aging at 60-90 °C. The core in our study was aged at 60 °C for >6 months, ensuring that the core sample wettability was restored to realistic reservoir wettability. The core properties and fluid saturations of the sample are presented in Table 3.

Table 1
FW ion content.

Ion	Concentration [ppm]
Na^+	6561
Cl^-	8716
$HCO3^-$	2684
K^+	64

Table 2
Fluid viscosities and densities.

Fluid	Viscosity [cp] @50 °C	Density [g cc−1]
Oil	4.4	0.856
FW	0.55	1.017
NF	0.60	1.020

2.2. Core flooding experiment

To mimic the reservoir conditions as much as possible, the core holder was surrounded by a heating jacket set to 50 °C, and a confining pressure of 2000 psi was applied. The core flooding experiment occurred in two stages: (1) FW was injected at a rate of 0.5 cc min^{-1}; and (2) FW injection switched to NWAG injection when the water cut reached 100%. The NF injection rate was 0.5 cc min^{-1}, and the CO_2 injection rate was 1 cc min^{-1} at an NWAG ratio of 1:1, with two pore volumes each. The discharged liquids were collected in measuring cylinders, and production data were recorded. The core flooding experiment was utilized as the basis for the 1D laboratory-scale model. Since the pressure of the outlet was at atmospheric pressure, the CO_2 dissolution in the injected NF or formation water was minimal because of the small core volume, the short gas residence time inside the core, and the limited solubility of CO_2 at near-atmospheric pressure. Therefore, CO_2 solubility was considered negligible in the laboratory experiment.

Using a second core sample of the same type, the oil–water relative permeabilities were measured using the steady-state method. The resulting curves were fitted using Equations (1) and (2), representing Corey correlation models, to determine the values of exponents n_o and n_w.

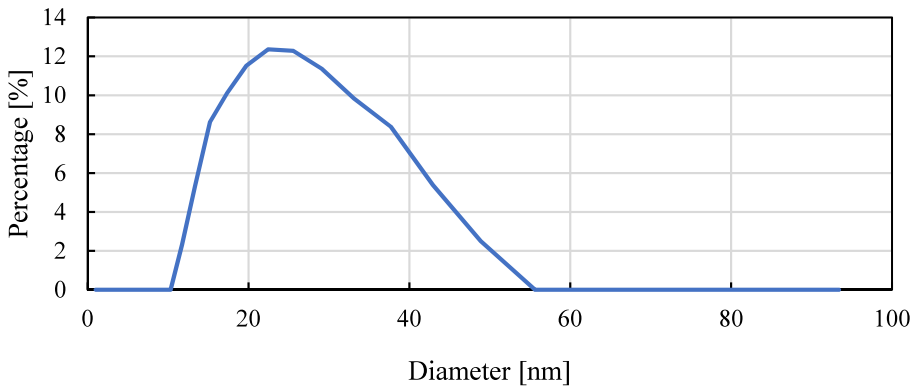

Fig. 2. SiO_2 NP size distribution.

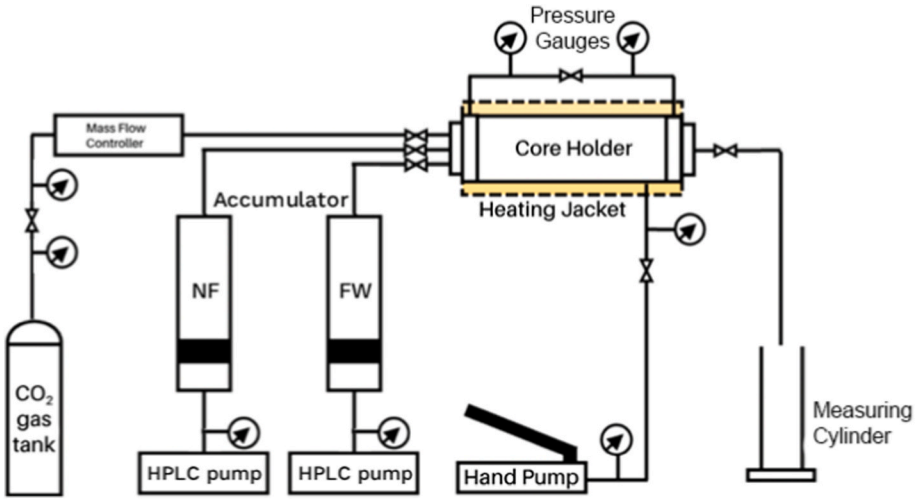

Fig. 3. SRP350 core flooding apparatus.

Table 3
Properties and fluid saturations of sandstone core sample.

Property	Unit	Value
Diameter	mm	75.846
Length	mm	38.04
Porosity	-	0.2211
Permeability	mD	401.7
Oil saturation	-	0.6511
Water saturation	-	0.3489

$$k_{ro} = (k_{ro})_{S_{wc}} \left(\frac{1 - S_w - S_{orw}}{1 - S_{wc} - S_{orw}} \right)^{n_o} \quad (1)$$

$$k_{rw} = (k_{rw})_{S_{orw}} \left(\frac{S_w - S_{wc}}{1 - S_{wc} - S_{orw}} \right)^{n_w} \quad (2)$$

where k_{ro} and k_{rw} denoted the relative permeabilities of oil and water, respectively; $(k_{ro})_{S_{wc}}$ and $(k_{rw})_{S_{or}}$ represent the relative permeabilities of oil and water at the endpoints of the curves, respectively; S_w denotes the water saturation; S_{wc} refers to the connate water saturation; S_{orw} refers to the residual oil saturation; and the exponents n_o and n_w represent the nonlinearity of the relative permeability curves of oil and water, respectively. (Ahmed, 2018) These equations were adopted to generate the relative permeability curves for the core sample used in the NWAG flooding experiment.

Finally, using a third core sample, the gas saturations during imbibition and drainage were measured for hysteresis calculations using Land's trapping model. In this model, the trapped gas saturation is calculated using Equation (3).

$$S_{gt} = \frac{S_{gi}}{1 + CS_{gi}} \quad (3)$$

where S_{gi} denotes the gas saturation at the start of water injection and C refers to the Land's trapping coefficient calculated using Equation (4):

$$C = \frac{1}{S_{gtmax}} - \frac{1}{S_{gmax}} \quad (4)$$

where S_{gmax} denotes the maximum gas saturation, and S_{gtmax} represents the maximum trapped gas saturation during imbibition. (Juanes et al., 2006; Spiteri, 2005)

2.3. NP adsorption

The NP adsorption amount must be determined prior to performing simulations. In this study, the method described by (Yu et al., 2012) was adopted to measure NP adsorption. As shown in Figs. 4 and 5 g of sandstone powder was added to a beaker, followed by 400 g of NF, and they were constantly mixed. Samples were collected periodically, and the NP concentration in NF samples was monitored for 10 h using a Microwave Plasma Atomic Emission Spectrometer (Agilent Technology, Santa Clara, CA, USA). Since the materials are SiO_2 NPs and sandstone, the adsorption equilibrium was expected to take only a few hours to be reached (Yu et al., 2012). During sample collection, mixing was stopped for approximately 10 min to allow the sandstone powder to settle to avoid interference during measurements.

NP adsorption was calculated using Equations (5)–(7) (Hendraningrat et al., 2021).

$$W_{adsorbed\ NPs} = W_{NPs\ (initial)} - W_{NPs\ (final)} \quad (5)$$

$$Ads_{exp} = \frac{W_{adsorbed\ NPs}}{W_{sandstone\ powder}} \quad (6)$$

$$Ads_{model} = \frac{Ads_{exp} * \rho_{rock} * (1 - \varphi)}{\varphi * M_{SiO_2} * 10^6} \quad (7)$$

where W denotes the weight of NPs [mg] and sandstone powder [g]; Ads_{exp} refers to NP adsorption, as measured in the experiment [mg g^{-1}]; Ads_{model} refers to NP adsorption, as employed in the simulation model [gmol cc^{-1}]; ρ_{rock} denotes the rock density [g cc^{-1}]; M_{SiO2} refers to the molecular weight of NPs [kg mol^{-1}]; and φ denotes rock porosity.

2.4. One-dimensional laboratory-scale model

CMG STARS (CMG Ltd., Calgary, AB, Canada) was employed in the simulations. A summary of STARS governing equations is presented in Table 4 (CMG STARS User Manual; Tai and Gates, 2024). The 1D model comprised 75 blocks, and the properties were set to be equal to the core sample properties listed in Table 3. While the model possessed a square cross-section, the side length was set to make the cross-section area equal to the core sample's circular cross-section area. The temperature and injection scheme were the same as those in the core flooding experiment. To simulate NF injection, CMG Builder provides a process wizard named "Petronas AFM (Nano-Particles) Wizard" that enables automated integration of NP adsorption, the NF–oil relative permeabilities, and permeability damage in the simulation (Hendraningrat

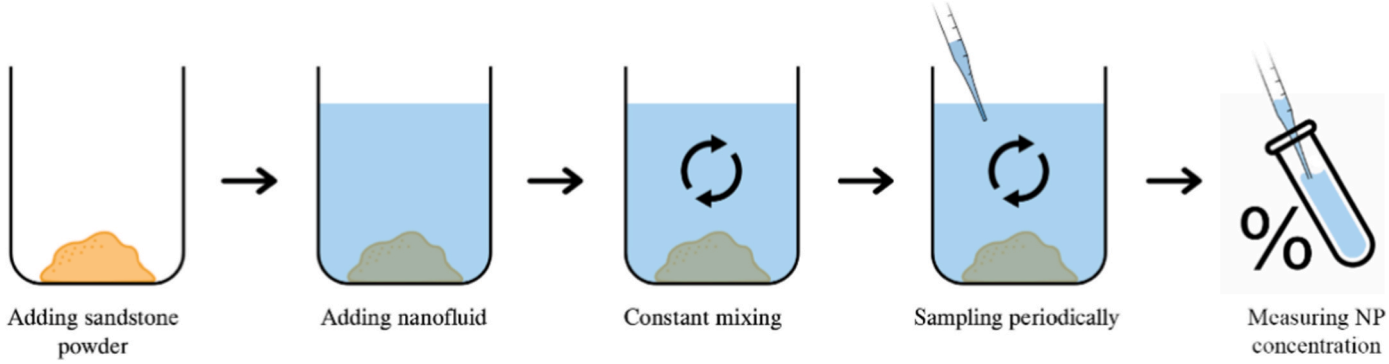

Fig. 4. Steps of measuring NP adsorption on sandstone.

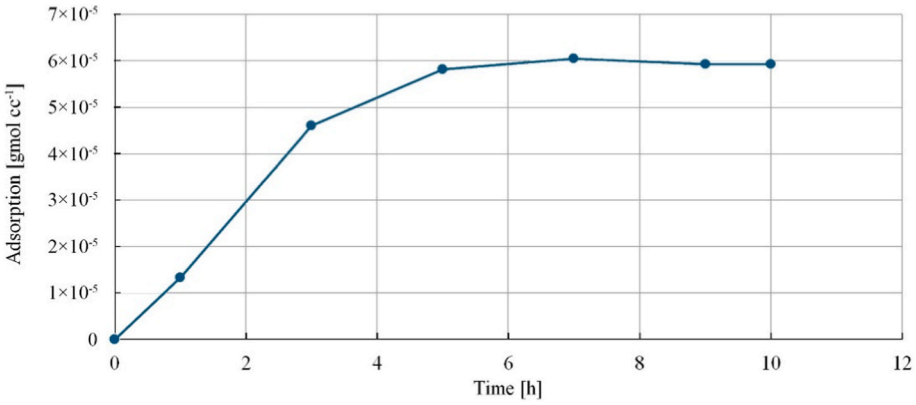

Fig. 5. SiO_2 NP adsorption over time on sandstone surface.

Table 4
Summary of STARS governing equations.

Equation name	Equation
Darcy's law	$u_* = -\frac{k_*}{\mu_*}\nabla\Phi_*$
Potential	$\Phi = g\,(z - z_{datum}) + \int_{P_{datum}}^{P} \frac{dP}{\rho}$
Mass balance	$\frac{\partial}{\partial t}\left[V_f(\rho_w S_w w_i + \rho_o S_o x_i + \rho_g S_g y_i) + V_v\, Ad_i\right] = \sum_{k=1}^{n_f}\left[T_w\rho_w w_i\Delta\Phi_w + T_o\rho_o x_i\Delta\Phi_o + T_g\rho_g y_i\Delta\Phi_g\right] + V\sum_{k=1}^{n_r}(s'_{ki} - s_{ki})r_k + \sum_{k=i}^{n_f}\left[\varphi\, D_{wi}\rho_w\Delta w_i + \varphi\, D_{oi}\rho_o\Delta x_i + \varphi\, D_{gi}\rho_g\Delta y_i\right] + \delta_{iw}\sum_{k=1}^{n_f}\rho_w q_a q_{wk} + \rho_w q_{wk} w_i + \rho_o q_{ok} x_i + \rho_g q_{gk} y_i$ [well layer k]
Phase saturation constraint	$S_w + S_o + S_g = 1$
Phase pressure constraint	$p_w = p_o - p_{cow(S_w)}$ $p_g = p_o + p_{cog(s_g)}$
Permeability reduction factor	$RK = 1.0 + (RRF - 1.0)\, Ad/AdMAXT$

u_*: velocity of phase *; k_*: effective permeability; μ_*: viscosity; $\nabla\Phi_*$: potential gradient; z: elevation above the datum location; P: pressure; ρ: density; S: saturation; i: component index; n_f: number of neighboring grid blocks; n_r: number of reactions; s': product stoichiometric coefficient; s: reactant stoichiometric coefficient; r: volumetric rate of reaction; w, x, y: component mass fractions in water, oil, gas phases, respectively; V_f: volume of fluid phases added together; V_v: void volume; Ad: adsorption term; T: transmissibility between the two regions; D: dispersion coefficient; δ_{iw}: Kronecker delta; $\partial/\partial t$: time derivative; P_c: capillary pressure; RK: permeability reduction factor; RRF: region dependent resistance factor; AdMAXT: Maximum adsorption level.

et al., 2021). The process wizard works only with STARS, making it the ideal choice to use for an NWAG simulation. The NF–oil relative permeabilities were derived from changes in residual oil saturation reduction induced by NF and changes in water relative permeability, which was calculated using the Darcy correlation. The 3-phase relative permeabilities were determined using CMG CMOST by adjusting the gas relative permeability to achieve the best possible match with the experimental results. The maximum trapped gas saturation was calculated using Equation (1) and then adopted in the hysteresis simulation. Finally, rock compressibility (C_f) was set at 8.75 × 10^{-6} psi^{-1} after estimating it using Equation (8) (Ganat et al., 2024):

$$C_f\left[psi^{-1}\right] = \left(-5786.5\varphi^3 + 4956.2\varphi^2 - 1407.9\varphi + 140.3\right)10^{-6} \quad (8)$$

After completing the simulation, the agreement between the experimental and simulated results or between simulation runs was evaluated using the coefficient of determination (R^2) and Root Mean Square Error (RMSE) computed as shown in Equations (9) and (10), respectively:

$$R^2 = 1 - \frac{\sum_{i=1}^{n}(x_i - y_i)^2}{\sum_{i=1}^{n}(x_i - \bar{x}_i)^2} \quad (9)$$

$$RMSE = \sqrt{\frac{1}{n}\sum_{i=1}^{n}(x_i - y_i)^2} \quad (10)$$

where n is the total number of values; x_i is the experimental value; y_i is the simulated value; and $\bar{x}_i$ is the mean of experimental values. (Abdellatief et al., 2025)

2.5. Three-dimensional reservoir-scale model

The reservoir-scale model was created by upscaling the 1D laboratory-scale model. The grid comprised 40 × 40 × 5 blocks, and each block measured 5 × 5 × 10 m. The reservoir was generally

homogenous, but slight variations in porosity and permeability were introduced for added realism, with the average porosity and permeability values across the reservoir being equal to those of the core sample. A 5-spot pattern was employed for well placement, with the production well in the center and four injection wells in the corners. The simulation parameters adopted for the reservoir-scale model are listed in Table 5. The duration of the simulation was set to 15 years, and the point of switching between FW and NWAG injections was at 99% water cut.

To maintain similar NP behaviors in reservoir- and laboratory-scale simulations, the reaction rates between NPs governing their aggregation and sedimentation were adjusted using upscaling factors, as expressed in Equations (11) and (12) (Hendraningrat et al., 2022). The rates for these reactions were determined using CMG CMOST in the same way as the gas relative permeability.

$$Upscale\ Factor = \frac{Reservoir\ scale\ grid\ size\ in\ i\ direction}{Laboratory\ scale\ grid\ size\ in\ i\ direction} \quad (11)$$

$$Upscaled\ reaction\ rate = \frac{Laboratory\ scale\ value}{Upscaling\ Factor} \quad (12)$$

Given that the CO_2 storage performance of NWAG injection was relevant, the effects of NPs on CO_2 absorption in NF was considered in the simulation, even though the simulation period was short and the soluble amount was small. According to (Rahmatmand et al., 2016), SiO_2 NF absorbed 21% more CO_2 than pure water, although their experiments involved lower pressure and NP concentrations than the reservoir model presented herein. However, in the same study, higher pressure and NP concentrations resulted in higher CO_2 absorption. Consequently, an absorption increase of 21% was employed herein as an estimate upon which to base the NF effect. The equilibrium constants for CO_2 in water under reservoir conditions were determined using CMG WinProp, then adjusted to increase absorption by 21% before their implementation in the model. The sensitivity to this parameter was low and removing it completely only resulted in a difference of ~1.3% in CO_2 storage. Therefore, if the estimation were slightly higher or lower than 21%, the impact on CO_2 storage would remain small. The amount of stored CO_2 in the reservoir was calculated by subtracting the amount of CO_2 produced from that injected to account for all kinds of trapping.

The parameters considered for sensitivity analysis were NWAG ratio, slug size, and NP concentration. Table 6 presents the considered values of each parameter. NF viscosity changed when altering the NP concentration, as shown in Table 7. The viscometer employed in the study only reported two decimals places, leading to the same viscosity values for 0.25 wt% and 0.1 wt% NF. Nevertheless, changes in NF viscosity at different NP concentrations were implemented during the simulation.

3. Results and discussion

3.1. NP adsorption

The Berea Buff sandstone core sample used in this study contained approximately 93% quartz, which is the same material as the NPs. They possess similar surface charges that create a repulsion force called the electric double layer force. However, the repulsion force is weakened and the Van der Waals attraction force is dominant under saline or high ionic strength conditions, facilitating SiO_2 NP adsorption on the sandstone surface (Chakraborty and Panigrahi, 2020; Esfandyari Bayat et al., 2015). Fig. 5 presents the NP adsorption over time, calculated using Equation (7). Maximum NP adsorption was reached after 5 h and remained stable until the end of the measurements. The average of the last three values, 5.98×10^{-5} gmol cc^{-1} was employed in the model as the maximum adsorption value (AdMAXT). Having NP adsorption occur over time during the simulation was only implemented for the laboratory-scale model; it was not required for the reservoir-scale model owing to the large timeframe. (CMG Builder User Manual, Petronas AFM (Nanoparticle) Wizard).

Table 5
Properties and simulation parameters of 3D reservoir-scale model.

Property	Unit	Value
Grid top depth	m	1000
Dimensions	m	200 × 200 × 50
Porosity	-	0.216–0.227
Permeability	mD	392–412
Pressure	MPa	10
Temperature	°C	50
Oil saturation	-	0.6511
Water saturation	-	0.3489

Table 6
Considered values of each parameter during sensitivity analysis.

Property	Values
Slug size [hydrocarbon pore volume, HCPV]	0.1, 0.2, 0.3, 0.4
NWAG ratio	3:1, 2:1, 1:1, 1:2, 1:3
NP concentration [wt%]	0.5, 0.25, 0.1, 0.05

Table 7
NF viscosity at different NP concentrations.

NP concentration [wt%]	Viscosity [cp] @50 °C
0.25	0.58
0.10	0.58
0.05	0.56

3.2. Relative permeabilities

After determining the values of n_w and n_o through steady-state relative permeability measurements, the FW–oil relative permeability curves in the simulation models were calculated using Equations (1) and (2), and the resulting curves are presented in Fig. 6. The crossing point between curves occurred at an S_w value of 0.64, indicating the water-wet state of the sandstone core sample. In the same figure, the NF–oil relative permeability curves derived using CMG tools are presented, and they show a small shift to the right, indicating a wettability shift toward more water-wet characteristics. The gas–liquid relative permeability was determined using CMG CMOST, and the 3-phase oil relative permeability is presented in Fig. 7. Finally, the Land's trapping coefficient and maximum trapped gas saturation during imbibition were calculated to be 4.13 and 0.1411 using Equations (4) and (3), respectively. The value of maximum trapped gas saturation was used as a required input in Builder for hysteresis simulation.

3.3. Core flooding experiment results

The results of the core flooding experiment, presented in Fig. 8, indicated oil recovery factors of 55.19% and 62.69% after FW and NWAG injection, respectively, representing an increase of 7.5%. The gas, water, and oil saturations at the end of the experiment were 0.3386, 0.4535, and 0.2079, respectively. Matching the experimental saturation values with the simulation values was important given that these values revealed how much gas was stored at the end of the process.

3.4. One-dimensional laboratory-scale simulation results

After implementing the laboratory measurements and calculated parameters, the simulation results closely matched the core flooding experiment results, as most oil recovery factor values fell within a 3% tolerance area, as shown in Fig. 9. The same figure also illustrates the fluid saturation results, and the differences between the experimental and simulation results were <0.01 for each fluid. The RMSE value for oil recovery factor curves was 0.01782, and for the saturations of gas, oil,

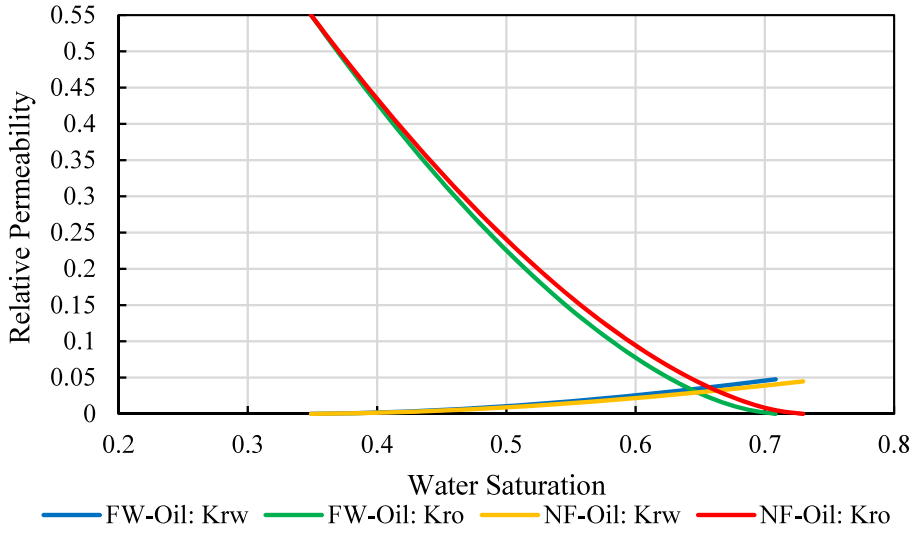

Fig. 6. FW–oil and NF–oil relative permeabilities in the simulation models.

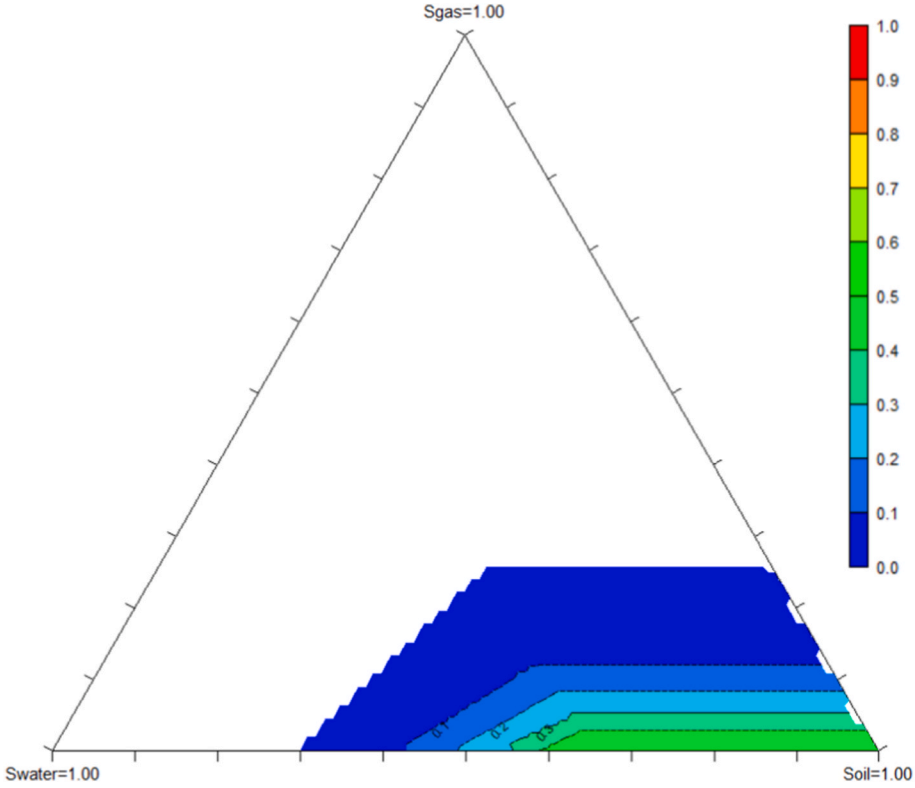

Fig. 7. Three-phase oil relative permeability.

and water, they were 0.0027, 0.0013, and 0.0040, respectively.

During NF injection, NPs adsorb on the sandstone surface and shift the relative permeabilities used by the simulator from FW–oil to NF–oil, improving oil recovery. After injection, NPs undergo aggregation and sedimentation reactions, leading to regional flow resistance (pore plugging effect) dependent on the amounts of sediment and adsorbed large NP clusters. This resistance creates divergent flow paths, further improving oil recovery.

3.5. Three-dimensional reservoir-scale simulation results

The laboratory-scale model was upscaled to the reservoir scale, as shown in Fig. 10. FW was injected for 6 years before reaching 99% water cut, and the system was switched to NWAG injection. The parameters listed in Table 6 were tested individually, beginning with slug size, with the NWAG ratio maintained at 2:1 for the sake of comparison. As shown in Fig. 11, the final oil recovery factor was almost the same at various slug sizes because oil saturation reached the critical point set in the simulation settings given enough time. However, the initial oil recovery factor was higher with smaller slug sizes, which was attributed to a more regular sweeping front for the gas given that the injection process alternated between NF and gas more frequently. These results aligned with those reported by (Hu et al., 2023) and (Ko et al., 2024), who concluded that smaller NWAG slugs led to better performance. In the 3D

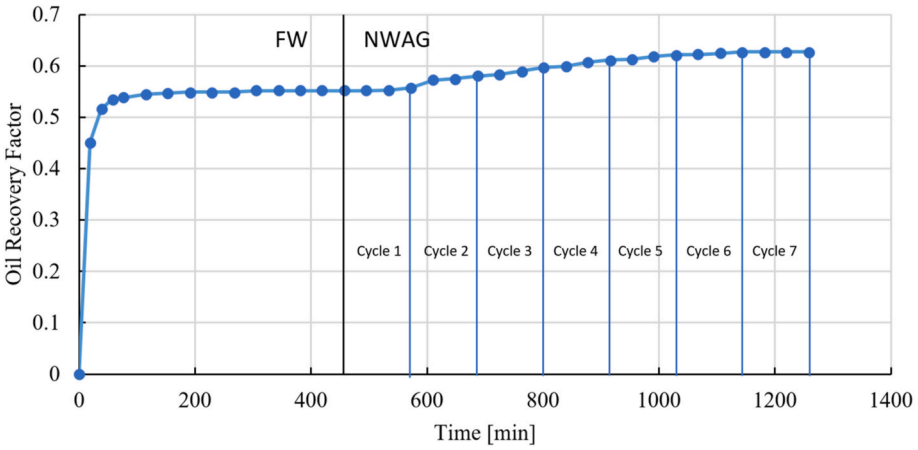

Fig. 8. Results of core flooding experiments: oil recovery factor for FW and NWAG injections at an NWAG ratio of 1:1.

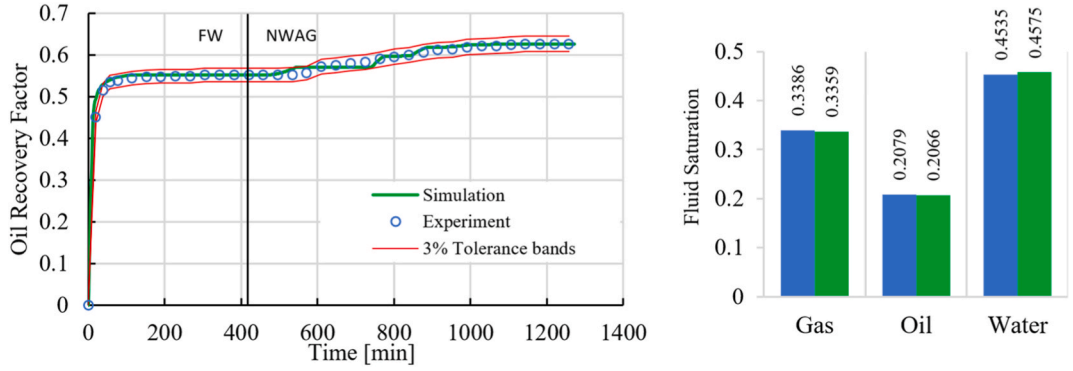

Fig. 9. Experimental and laboratory-scale simulation results of oil recovery factor and final fluid saturations.

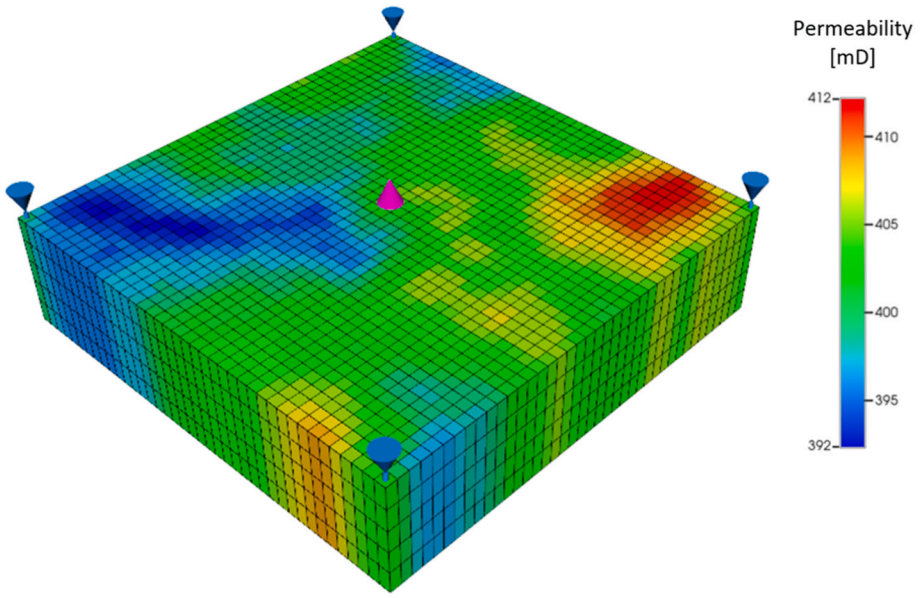

Fig. 10. Three-dimensional reservoir-scale model illustrating the locations of the production well (pink cone) and injection wells (blue cones) and the permeability distribution. (For interpretation of the references to colour in this figure legend, the reader is referred to the Web version of this article.)

reservoir-scale simulation, the oil recovery differences between slug sizes of 0.2 and 0.1 HCPV were negligible, and a slug size of 0.2 HCPV was selected for the remaining tests.

The results of varying the NWAG ratio are presented in Fig. 12. Similar to slug size, differences in oil recovery mainly occurred in the early stages of NWAG injection. The highest initial oil production rate was achieved using an NWAG ratio of 1:1, closely followed by 2:1. The injected NF enhanced the oil recovery by controlling gas mobility and

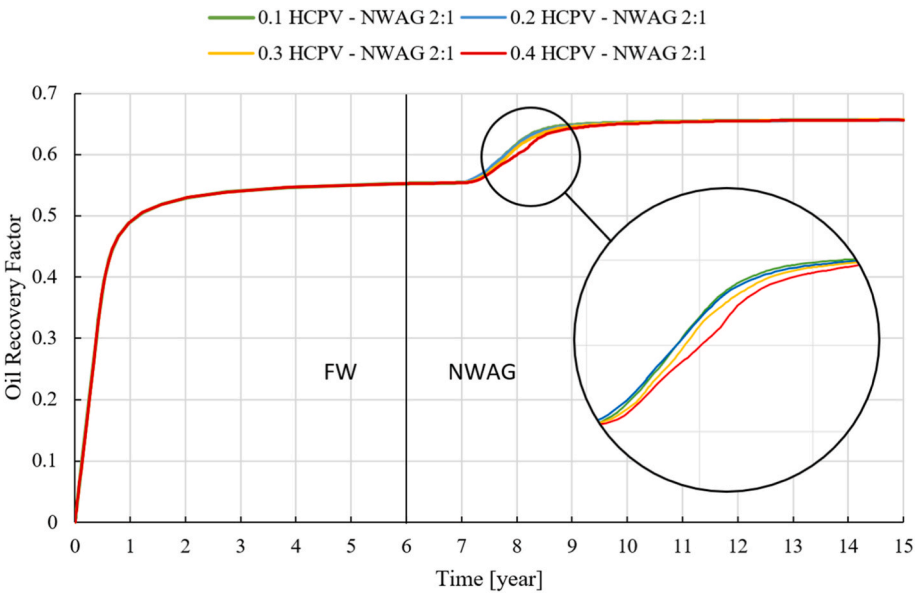

Fig. 11. Results of the three-dimensional reservoir-scale simulation showing oil recovery factors (fraction) vs time (years) at various slug sizes with an NWAG ratio of 2:1 and NP concentration of 0.5 wt%.

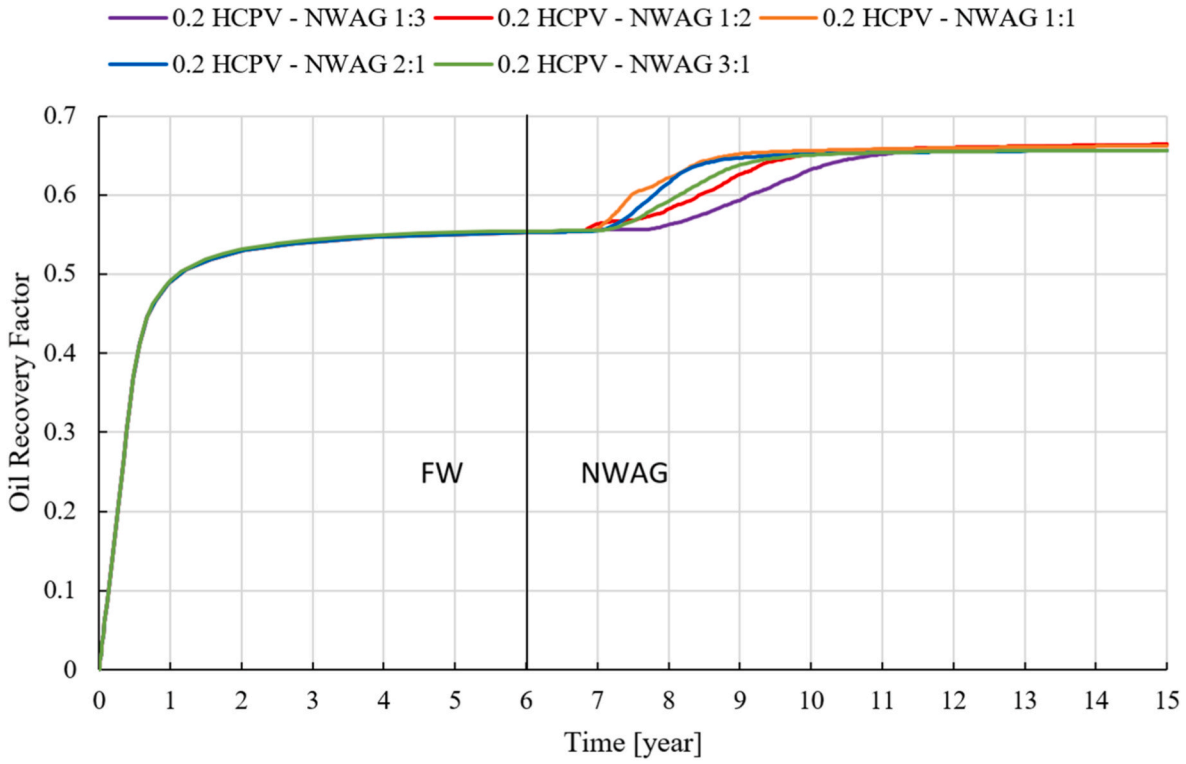

Fig. 12. Results of the three-dimensional reservoir-scale simulation showing oil recovery factor (fraction) vs time (years) at various NWAG ratios with a slug size of 0.2 HCPV and NP concentration of 0.5 wt%.

through its interaction with oil and sandstone. The gas sweeping efficiency was lower when the gas ratio was high, i.e., 1:2 and 1:3, resulting in slower oil recovery. Oil recovery from NF itself was not substantial, as shown in Fig. 6, given that only a slight alteration in wettability was induced by NF in the sandstone reservoir. Therefore, a high NF ratio resulted in slower oil recovery, although it remained faster than using a large gas ratio. A balance was struck at an NWAG ratio of 1:1, with an appropriate amount of injected NF synergizing improved oil recovery by controlling gas mobility and altering rock wettability. Additionally, a comparison between linear trend and average values of the mobility ratios in Block (i,j,k)=(10,10,1), located midway between an injection well and the production well, was performed. The results, presented in Fig. 13, show that high-gas ratios (1:3 and 1:2) exhibited the highest mobility ratios, confirming strong CO_2 override and poor sweep. High-NF ratios (3:1 and 2:1) achieved low mobility ratios but produced slower oil recovery due to insufficient gas drive. Finally, the 1:1 ratio maintained a lower mobility ratio compared to the high-gas cases, indicating more effective CO_2 mobility suppression, especially in the

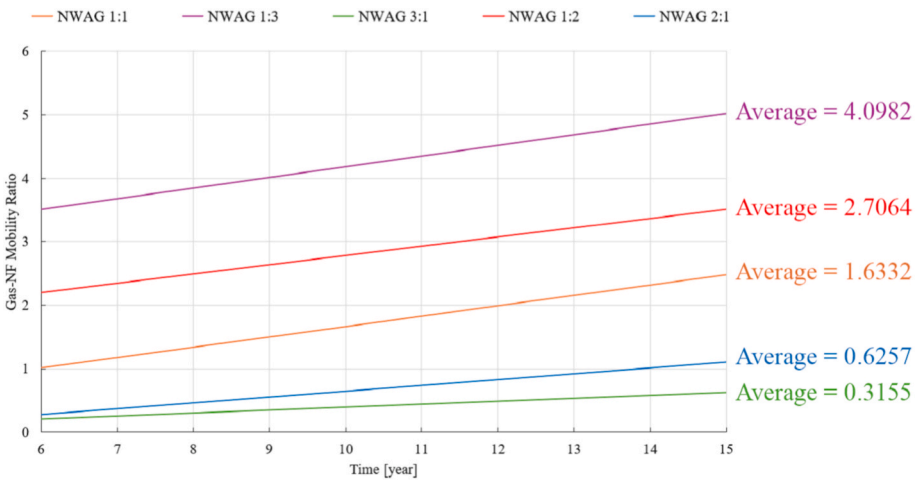

Fig. 13. Linear trend and average of gas mobility ratio in Block (10,10,1) at various NWAG ratios with a slug size of 0.2 HCPV and NP concentration of 0.5 wt%.

first few years, while still preserving sufficient gas injection for displacement. The mobility ratio trend in the 2:1 NWAG ratio case became better in later years, leading to the 1:1 and 2:1 NWAG ratio performances becoming almost identical after about 2.5 years of NWAG injection. Despite the close results, the 1:1 ratio was chosen as the optimal case due to the higher gas injection that enhances CO_2 storage.

Notably (Al Matroushi et al., 2015), and (Ko et al., 2024) concluded that NWAG ratios of 2:1 and 3:1, respectively, achieved more effective oil recovery. However, in both cases, NF substantially altered the wettability of the carbonate rock used in the simulations, changing from oil-wet to water-wet characteristics. In contrast (Hu et al., 2023), used sandstone in their experiments and concluded that a 1:1 NWAG ratio resulted in the best oil recovery performance.

Subsequently, a slug size of 0.2 HCPV and an NWAG ratio of 1:1 were employed to compare the effects of various NP concentrations on oil recovery. As shown in Fig. 14, the oil recovery factor was higher at an NP concentration of 0.5 wt% in the early stages of NWAG injection. Higher NP concentrations led to faster adsorption on the sandstone surface, with the effects on oil recovery observed earlier. However, the oil recovery effects at higher NP concentrations began to diminish beyond 0.25 wt%. The results of NP concentration effects agreed with those reported by (Ko et al., 2024).

The amounts of stored CO_2 across all variations are presented in Fig. 15. The slug size and NWAG ratio induced noticeable changes in CO_2 storage, whereas the NP concentration induced a negligible difference. In the case of slug size, a larger slug size resulted in a higher amount of stored CO_2. This finding was attributed to a higher gas volume being injected in each cycle, enabling higher gas saturation to be reached, especially in regions around the injection wells. As per Equation (3), higher gas saturation led to a greater volume of trapped gas during the imbibition cycle. Similar behavior was observed with the NWAG ratio, wherein higher gas ratios resulted in higher amounts of stored CO_2. Fig. 16 demonstrates an example of gas saturation distribution at the end of a high gas ratio and a high NF ratio cycles for comparison.

To validate the upscaling from 1D to 3D, a grid-sensitivity analysis was performed on the optimized case (slug size 0.2 HCPV, NWAG ratio 1:1, NP concentration 0.5 wt%). The original 3D reservoir model was refined by increasing the grid resolution by factors of 4 × and 8 × . Oil recovery results from the refined models were compared to the base case using RMSE and R^2, as summarized in Table 8. Regarding CO_2 storage performance, the difference between the final storage amount in base

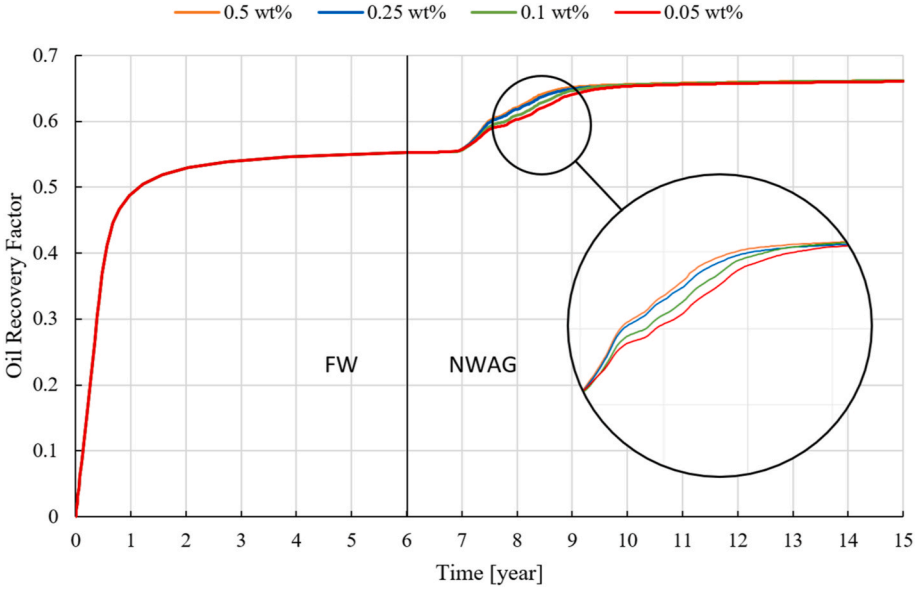

Fig. 14. Results of the three-dimensional reservoir-scale simulation showing oil recovery factor (fraction) vs time (years) at various NP concentrations with a slug size of 0.2 HCPV and an NWAG ratio of 1:1.

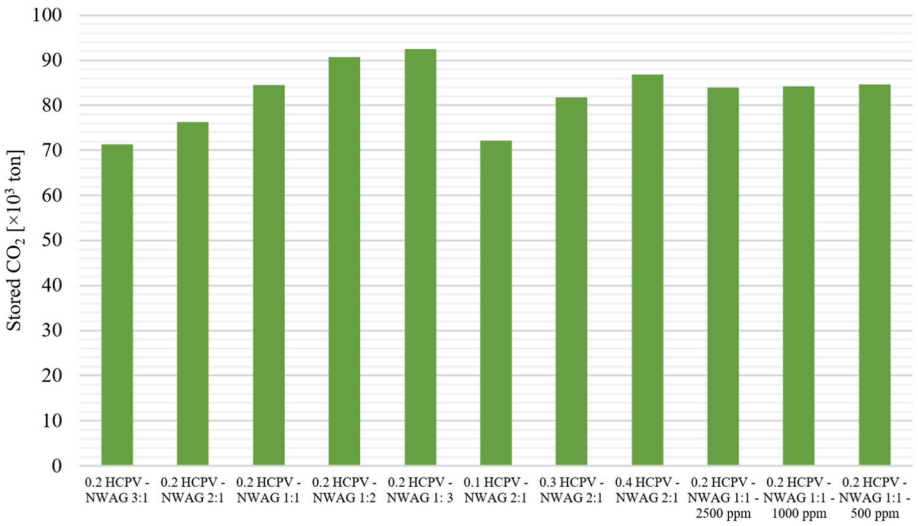

Fig. 15. CO_2 storage at different slug sizes, NWAG ratios, and NP concentrations.

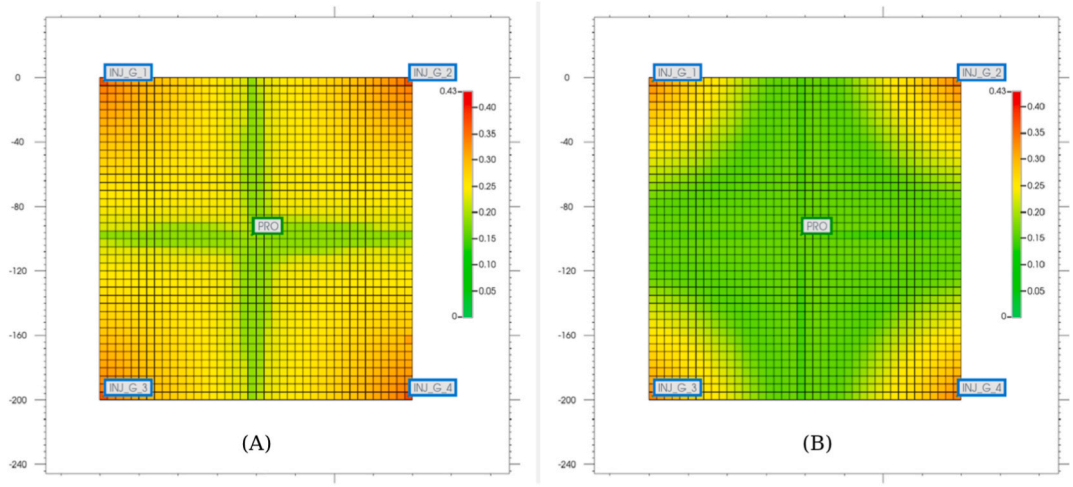

Fig. 16. CO_2 distribution comparison between a high-gas and high-NF ratio injections at the end of a cycle. (A): 0.2 HCPV slug size, 1:3 NWAG ratio, and 0.5 wt% NPs concentration. (B): 0.2 HCPV slug size, 3:1 NWAG ratio, and 0.5 wt% NPs concentration.

Table 8
RMSE and R^2 metrics comparing oil recovery performance between the original and refined grids of the reservoir scale model in the optimal case.

Comparison	RMSE	R^2
Base vs 4 × resolution	0.015289	0.992410
Base vs 8 × resolution	0.013266	0.994286

case and final storage amount in 4 × and 8 × cases was 0.97% and 2.22%, respectively. The grid refinement led to only minor variations in performance, indicating that the results are not artifacts of insufficient grid resolution and confirming the validity of the upscaling approach.

The CO_2 storage results were obtained at the end of the last NWAG cycle in each case. However, CO_2 storage is not linear over time, and, from an operational perspective, it would be inefficient to operate the NWAG injection process beyond the point where oil recovery starts being uneconomical. Assuming that this point occurs at 99% water cut, the operation would stop in the 3rd month of the 10th year, after 9 NWAG cycles, using the parameters that induced the fastest oil recovery (i.e., slug size of 0.2 HCPV, NWAG ratio of 1:1, and NP concentration of 0.5 wt%). The amount of stored CO_2 at that time would be 81.4 × 10^3 tons, providing an optimal way to operate the NWAG enhanced oil recovery process under the reservoir conditions simulated in this study.

4. Conclusions

Enhanced oil recovery through NWAG injection has proven its potential in multiple studies. However, performing sensitivity analysis for its many crucial parameters is necessary via simulations. Several studies reported simulations of NWAG injection in carbonate reservoirs. This study presents a 3D reservoir-scale simulation of NWAG injection using SiO_2 NPs and CO_2 gas to determine the effects of slug size, NWAG ratio, and NP concentration on oil recovery and CO_2 storage performance in a sandstone reservoir. The simulation was conducted using CMG software by upscaling a 1D laboratory-scale model, which was matched to a core flooding experiment. Results revealed that larger slug sizes resulted in lower oil recovery in the initial stages of NWAG injection; however, a slug size smaller than 0.2 HCPV did not lead to noticeable improvement. This finding was attributed to higher-frequency switching between NF and gas injections, leading to more controlled gas flow and a more regulated sweeping front. Higher NF or gas ratios resulted in inferior oil production performance compared to a balanced 1:1 NWAG ratio. The result was attributed to NF injection itself improving oil recovery and simultaneously controlling gas flow. By contrast, the 1:1 NWAG ratio

resulted in an appropriate amount of NF injection to synergize these dual roles. Moreover, results demonstrated that higher NP concentrations led to faster adsorption on the sandstone surface and higher NF viscosity, enhancing oil production performance. The CO_2 storage results indicated that larger slugs and a higher gas ratio resulted in higher CO_2 storage capacity in the sandstone reservoir due to higher trapped gas saturation. To achieve more practical and efficient operation, a slug size of 0.2 HCPV, an NWAG ratio of 1:1, and NP concentration of 0.5 wt% for nine cycles over 10 years and 3 months are suggested to achieve optimum oil recovery and CO_2 storage in a sandstone reservoir under the described conditions.

Notably, this study was limited to the upscaled version of a 1D model of a core flooding experiment, making the simulation accuracy and credibility for the reservoir scale far from ideal. The analysis would be greatly improved by using a more detailed simulation with real reservoir data where NWAG or at least NF injection was conducted. Additionally, because the reservoir mentioned here is a generic reservoir, key inputs for economic evaluation—such as injection/production strategy, local CO_2 transport and compression costs, regional silica NPs pricing, and the applicable CO_2 credit or storage incentives—cannot be reliably determined as they vary greatly by case. Therefore, any economic assessment presented here would not be generalizable. This limitation can also be addressed by making a simulation using real data of a specific reservoir.

CRediT authorship contribution statement

Ragheed Alali: Writing – original draft, Conceptualization. **Kazunori Abe:** Writing – review & editing, Supervision, Funding acquisition. **Hikari Fujii:** Supervision, Funding acquisition.

Declaration of competing interest

The authors declare that they have no known competing financial interests or personal relationships that could have appeared to influence the work reported in this paper.

Acknowledgement

This work was supported by JSPS KAKENHI Grant Number JP24K08317.

Appendix A. Supplementary data

Supplementary data to this article can be found online at https://doi.org/10.1016/j.geoen.2026.214433.

Data availability

Data will be made available on request.

References

Abdellatief, M., Elsafi, M., Murali, G., ElNemr, A., 2025. Comparative evaluation of hybrid machine learning models for predicting the strength of metakaolin-based geopolymer concrete enhanced with Gaussian noise augmentation. J. Build. Eng., 113302

Abdulsada, J.A., Chen, H., Wei, B., Ren, Y., 2025. A mini-review of Water-alternating-CO2 injection process and derivations for enhanced oil recovery and CO2 storage in subsurface reservoirs. Petroleum 11 (4), 410–421.

Abe, K., Negishi, K., Fujii, H., 2023. Experimental investigation of the effects of the sizes and concentrations of SiO2 nanoparticles on wettability alteration and oil recovery. Energy & Fuels 37 (10), 7122–7129.

Ahmed, T., 2018. Reservoir Engineering Handbook. Gulf professional publishing.

Al-Ameer, M.A., Azad, M.S., Al-Shehri, D., Mahmoud, M., Kamal, M.S., Patil, S., 2023. A guide for selection of aging time and temperature for wettability alteration in various rock-oil systems. ACS Omega 8 (34), 30790–30801.

Al Matroushi, M., Pourafshary, P., Al Wahaibi, Y., 2015. Possibility of nanofluid/gas alternating injection as an EOR method in an oil field. In: Abu Dhabi International Petroleum Exhibition and Conference.

Alali, R., Abe, K., Seddiqi, K.N., Fujii, H., 2023. Effect of carbon dioxide injection on limestone permeability damage induced by alumina nanoparticles for enhanced oil recovery applications. Appl. Sci. 13 (13), 7446.

Alsaba, M.T., Al Dushaishi, M.F., Abbas, A.K., 2020. A comprehensive review of nanoparticles applications in the oil and gas industry. J. Pet. Explor. Prod. Technol. 10, 1389–1399.

Aziz, H., Muther, T., Khan, M.J., Syed, F.I., 2021. A review on nanofluid water alternating gas (N-WAG): application, preparation, mechanism, and challenges. Arabian J. Geosci. 14 (14), 1416.

Cao, C., Song, Z., Su, S., Tang, Z., Xie, Z., Chang, X., Shen, P., 2021. Water-based nanofluid-alternating-CO2 injection for enhancing heavy oil recovery: considering oil-nanofluid emulsification. J. Petrol. Sci. Eng. 205, 108934.

Chakraborty, S., Panigrahi, P.K., 2020. Stability of nanofluid: a review. Appl. Therm. Eng. 174, 115259.

CMG builder user manual, petronas AFM (nanoparticle) wizard. In. (Version 2025.10) Computer Modelling Group Ltd.

CMG STARS user manual. In. Computer Modelling Group Ltd.

Deshmukh, M., Pathan, A., 2025. Advancements and challenges in the use of surfactants and nanoparticles for enhanced oil recovery: mechanisms, synergies, and field applications. Environ. Sci. Pollut. Control Ser. 1–35.

Ehtesabi, H., Ahadian, M.M., Taghikhani, V., Ghazanfari, M.H., 2014. Enhanced heavy oil recovery in sandstone cores using TiO2 nanofluids. Energy & Fuels 28 (1), 423–430.

Esfandyari Bayat, A., Junin, R., Samsuri, A., Piroozian, A., Hokmabadi, M., 2014. Impact of metal oxide nanoparticles on enhanced oil recovery from limestone media at several temperatures. Energy & Fuels 28 (10), 6255–6266.

Esfandyari Bayat, A., Junin, R., Shamshirband, S., Tong Chong, W., 2015. Transport and retention of engineered Al2O3, TiO2 and SiO2 nanoparticles through various sedimentary rocks. Sci. Rep. 5 (1), 14264.

Fang, P., Zhang, Q., Zhou, C., Yang, Z., Yu, H., Du, M., Chen, X., Song, Y., Wang, S., Gao, Y., 2024. Chemical-assisted CO2 water-alternating-gas injection for enhanced sweep efficiency in CO2-EOR. Molecules 29 (16), 3978.

Ganat, T., Hrairi, M., Badawy, A., Khosravi, V., Abdalla, M., 2024. Advancing sandstone reservoir compressibility prediction: a correlation-driven methodology. Petroleum Research 9 (2), 273–279.

Hendraningrat, L., Majidaie, S., Kechut, N.I., Tewari, R.D., Sedaralit, M.F., Skoreyko, F., MousaviMirkalaei, S.M., Edmondson, M., Chandrasekar, V., 2022. Application of novel advanced numerical modeling of nanoparticles for improved oil recovery: Laboratory-to field-scale. In: SPE Annual Technical Conference and Exhibition?.

Hendraningrat, L., Majidaie, S., Ketchut, N.I., Skoreyko, F., MousaviMirkalaei, S.M., 2021. Advanced reservoir simulation: a novel robust modelling of nanoparticles for improved oil recovery. In: SPE Annual Technical Conference and Exhibition?.

Hogeweg, A.S., Hincapie, R.E., Foedisch, H., Ganzer, L., 2018. Evaluation of aluminium oxide and titanium dioxide nanoparticles for EOR applications. In: SPE Europec Featured at 80th EAGE Conference and Exhibition.

Hu, J., Fu, M., Li, M., He, H., Hou, B., Chen, L., Liu, W., 2023. Study on SiO2 nanofluid alternating CO2 enhanced oil recovery in low-permeability sandstone reservoirs. Processes 11 (9), 2758.

IEA, T.I.E.A., 2024. World energy outlook 2024. https://www.iea.org/reports/world-energy-outlook-2024. (Accessed 4 August 2025).

Juanes, R., Spiteri, E., Orr Jr, F., Blunt, M., 2006. Impact of relative permeability hysteresis on geological CO2 storage. Water Resour. Res. 42 (12).

Kandiel, Y.E., Attia, G.M., Metwalli, F.I., Khalaf, R.E., Mahmoud, O., 2025. Nanoparticles in enhanced oil recovery: State-of-the-art review. J. Pet. Explor. Prod. Technol. 15 (4), 66.

Ko, S., Park, H., Jang, H., 2024. Nano-water-alternating-gas simulation study considering rock–fluid interaction in heterogeneous carbonate reservoirs. Energies 17 (19), 4846.

Kumasaka, J., Kaito, Y., Goto, A., Ito, D., Kitagawa, H., Nogami, T., Murakami, S., 2024. First nanoparticle-based EOR project in Japan: field pilot test. In: SPE Improved Oil Recovery Conference?.

Liang, F., Wang, W., Zhu, S., Hu, Y., Zhao, Z., Tan, Y., Yu, G., Hou, J., Li, J., 2025. Nanofluids application in enhanced oil recovery process-opportunities and challenges. Arab. J. Chem. 18 (1), 106053.

Luo, P., Luo, W., Li, S., 2017. Effectiveness of miscible and immiscible gas flooding in recovering tight oil from Bakken reservoirs in Saskatchewan, Canada. Fuel 208, 626–636.

Moradi, B., Pourafshary, P., Jalali, F., Mohammadi, M., Emadi, M.A., 2015. Experimental study of water-based nanofluid alternating gas injection as a novel enhanced oil-recovery method in oil-wet carbonate reservoirs. J. Nat. Gas Sci. Eng. 27, 64–73. https://doi.org/10.1016/j.jngse.2015.07.009.

Ogolo, N.A., Olafuyi, O., Onyekonwu, M., 2012. Enhanced oil recovery using nanoparticles. In: SPE Kingdom of Saudi Arabia Annual Technical Symposium and Exhibition.

Rahmatmand, B., Keshavarz, P., Ayatollahi, S., 2016. Study of absorption enhancement of CO2 by SiO2, Al2O3, CNT, and Fe3O4 nanoparticles in water and amine solutions. J. Chem. Eng. Data 61 (4), 1378–1387.

Ren, D., Wang, X., Kou, Z., Wang, S., Wang, H., Wang, X., Tang, Y., Jiao, Z., Zhou, D., Zhang, R., 2023. Feasibility evaluation of CO2 EOR and storage in tight oil reservoirs: a demonstration project in the Ordos Basin. Fuel 331, 125652.

Spiteri, E.J., 2005. Relative permeability hysteresis: a new model and impact on reservoir simulation. In: The Degree of Master of Science Stanford.

Sun, X., Ning, H., Chen, G., Yu, G., Jia, Z., Zhang, Y., 2024. Experimental study of hybrid nanofluid-alternating-CO2 microbubble injection as a novel method for enhancing heavy oil recovery. J. Mol. Liq. 395, 123835.

Sun, X., Ning, H., Shi, Y., Yu, G., Jia, Z., Han, M., Zhang, Y., 2023. Study of CO2 solubility enhancement by nanomaterials in carbonated water: implications for enhanced oil recovery and CO2 storage. J. Clean. Prod. 396, 136562.
Tai, N., Gates, I.D., 2024. Cyclic CO2 storage and geothermal energy extraction using a huff and puff technique in the basal Cambrian sandstone unit, Canada. Geothermics 118, 102925.
Vittoni, C., Gatti, G., Paul, G., Mangano, E., Brandani, S., Bisio, C., Marchese, L., 2019. Non-porous versus mesoporous siliceous materials for CO2 capture. ChemistryOpen 8 (6), 719–727.
Yu, J., An, C., Mo, D., Liu, N., Lee, R., 2012. Study of adsorption and transportation behavior of nanoparticles in three different porous media. In: SPE Improved Oil Recovery Conference?.
Zhang, J., Zhao, Z., Xu, Z., Zhang, X., Zhang, L., 2023. Surface wettability of sandstone and shale: implication for CO2 storage. Int. J. Greenh. Gas Control 126, 103917.